Superconductivity and magnetic short-range order in the system with a Pd sheet sandwiched between graphene sheets

2004 J. Phys.: Condens. Matter 16 903

(http://iopscience.iop.org/0953-8984/16/6/018)

INSTITUTE OF PHYSICS PUBLISHING JOURNAL OF PHYSICS: CONDENSED MATTER

J. Phys.: Condens. Matter **16** (2004) 903–918 PII: S0953-8984(04)66949-9

Superconductivity and magnetic short-range order in the system with a Pd sheet sandwiched between graphene sheets

Masatsugu Suzuki[1], **Itsuko S Suzuki**[1] **and Jürgen Walter**[1,2]

[1] Department of Physics, State University of New York at Binghamton, Binghamton, NY 13902-6016, USA
[2] Department of Materials Science and Processing, Graduate School of Engineering, Osaka University, 2-1, Yamada-oka, Suita 565-0879, Japan

E-mail: suzuki@binghamton.edu (Masatsugu Suzuki) and Juerg_Walter@t-online.de

Received 23 July 2003, in final form 5 January 2004
Published 30 January 2004
Online at stacks.iop.org/JPhysCM/16/903 (DOI: 10.1088/0953-8984/16/6/018)

Abstract

Pd-metal graphite (Pd-MG) has a layered structure, where each Pd sheet is sandwiched between adjacent graphene sheets. The DC magnetization and AC magnetic susceptibility of Pd-MG have been measured using a SQUID magnetometer. Pd-MG undergoes a superconducting transition at T_c (=3.63 ± 0.04 K). The superconductivity occurs in the Pd sheets. The irreversibility between χ_{ZFC} and χ_{FC} occurs well above T_c. The susceptibility χ_{FC} obeys a Curie–Weiss behaviour with a negative Curie–Weiss temperature ($-13.1 \leqslant \Theta \leqslant -5.4$ K). The growth of magnetic order is limited by the disordered nature of nanographites, forming magnetic short-range order at low temperature in the graphene sheets.

(Some figures in this article are in colour only in the electronic version)

1. Introduction

Magnetism and superconductivity are manifestations of two different ordered states into which metals can condense at low temperatures. In general these two states are mutually exclusive; they do not coexist at the same site in the system. The study of the interplay between these properties has recently been revitalized by the discovery of a family of high-T_c boride carbides RNi_2B_2C (where R is a rare-earth element) [1, 2]. The R–C layers separated by Ni_2B_2 sheets are antiferromagnetically ordered below a Néel temperature T_N, while the Ni_2B_2 sheets are superconducting below T_c. Like RNi_2B_2C, Pd-metal graphite (MG) has a layered structure [3–7]. Ideally, a Pd monolayer is sandwiched between adjacent graphite sheets, forming a periodic c-axis stacking like graphite intercalation compounds (GICs). Each Pd layer consists of small islands formed of Pd nanoparticles with finite sizes. Pd nanoparticles would generate internal stress inside the graphite lattice, leading to the break up of adjacent graphene sheets into

nanographites. It is expected that the superconductivity occurs in Pd sheets and that the magnetic short-range order occurs in nanographites in graphene sheets.

In the present work, we have undertaken an extensive study on the magnetic properties of Pd-MG from various kinds of measurement using a SQUID magnetometer: the DC magnetization in the zero-field cooled (ZFC), field-cooled (FC), thermoremnant (TR), and isothermal remnant (IR) states, and the AC magnetic susceptibility (the dispersion and absorption). We show that this compound undergoes a superconducting transition at a critical temperature T_c ($=3.63 \pm 0.04$ K). The superconductivity occurs in the Pd sheets. The FC susceptibility well above T_c obeys a Curie–Weiss behaviour with a negative Curie–Weiss temperature Θ. The deviation of the ZFC susceptibility from the FC susceptibility starts to occur even at 298 K. These results suggest that a magnetic short-range order appears well above T_c. Based on these results, we propose a model that the superconductivity occurs in the Pd sheets and that the magnetic short-range order occurs in the graphene sheets. Although no long-range magnetic order below T_c has been clearly confirmed from the present work, it is assumed that the possible interplay between the superconductivity and the magnetic short-range order becomes significant below T_c.

Here we present experimental and theoretical backgrounds for the origin of the superconductivity in the Pd sheets and the magnetism in nanographites. The absence of superconductivity in pristine Pd above 2 mK is mainly due to strong spin fluctuations [8]. Theoretically it is suggested that Pd without spin fluctuations should be a superconductor [9, 10]. Experimentally, Stritzker [11] has reported that pure Pd films, evaporated between 4.2 and 300 K, can be transformed into superconductors by means of irradiation at low temperatures with He^+ ions. The maximum transition temperature obtained is 3.2 K. A special kind of disorder produced by low-temperature irradiation may lead to a smearing of the Fermi energy E_F, and thus to a reduction of the density of states (DOS) at E_F, $N(E_F)$. This reduction of $N(E_F)$ leads to a decrease in the Stoner enhancement factor. As a result, the strong spin fluctuations would be reduced and superconductivity might be possible. In fact, Meyer and Stritzker [12] have shown that the AC magnetic susceptibility of low-temperature irradiated Pd is strongly reduced in comparison to the annealed Pd metal.

Nanographites are nanometre-sized graphite fragments, forming a new class of mesoscopic system. Fujita *et al* [13] and Wakabayashi *et al* [14] have theoretically suggested that the electronic structures of finite-size graphene sheets depend crucially on the shape of their edges. Finite graphite systems having zigzag edges exhibit a special edge state. The corresponding energy bands are almost flat at E_F, giving a sharp peak in $N(E_F)$. The conduction electrons localized near the zigzag edge have magnetic moments ($=g\mu_B S$ with $g = 2$ and $S = 1/2$). Harigaya [15–17] has theoretically predicted that the magnetism in nanographites with zigzag edge sites depends on the stacking sequence of nanographites. The structure of pristine graphite consists of hexagonal net planes of carbon stacked along the *c* axis in a staggered array usually denoted as ABAB... [18]. There is a lateral shift on going from layer A to layer B. There are two kinds of spin configurations depending on the stacking of nanographites. For the A–B stacking, there is no interlayer interaction at the edge site, giving rise an antiferromagnetic (AF) spin alignment. The growth of AF spin order is greatly limited by the disordered nature of nanographites, forming magnetic short-range order. For the A–A type stacking, on the other hand, the magnetic moment per layer does not appear due to the interlayer interaction.

2. Experimental procedure

In a previous work [7] we have shown that there are two types of Pd-MG depending on the reduction condition in the sample preparation: long-reaction time and short-reaction time.

The physical properties of these two systems are rather different: ferromagnetic nature for the long-reaction time and AF nature for the short-reaction time. The sample used in the present work (the short-reaction time) is the same as that used in the previous work [7]. Pd-MG samples based on natural graphite were prepared by heating $PdCl_2$ GIC with mixed stages (2, 3, and 4) at 350 °C under hydrogen gas (flow rate 300 ml min^{-1}) for 2 h.

The detail of sample characterization for Pd-MG was presented in previous papers [3, 5]. The average size of Pd nanoparticles was estimated as (530 ± 340) Å from a bright field transmission electron microscope photograph [3]. The existence of nanographites was confirmed from the Raman scattering [5]. The Raman spectrum shows a large peak at 1580 cm^{-1} assigned as the E_{2g2} mode in pristine graphite (1582 cm^{-1}), and a small peak at 1360 cm^{-1} assigned as the D-band (disordered induced modes) of graphite [5]. The size of nanographites can be estimated from an empirical law $L_a = 4.4 \times I_{1580}/I_{1350}$, where I_{1580} and I_{1360} are the intensities of the corresponding peaks. In fact, the size of nanographites is of the same order as that of Pd nanoparticles. There is no appreciable charge transfer between nanographites and Pd nanoparticles.

The Pd-MG sample consists of many small flakes. Each flake has a well-defined c axis. If these flakes are carefully piled inside the sample capsule for the measurement, the c axis of the whole sample could correspond to the c axis of each flake. This is not the case for the present experiment. The present sample may be regarded as a powdered sample with the c axis randomly distributed over all directions. Because of the small samples, the resistivity measurement could not be carried out. The mass of the sample used in the present work was 23.8 mg.

The DC magnetization and AC magnetic susceptibility of Pd-MG were measured using a SQUID magnetometer (Quantum Design, MPMS XL-5). Before setting up a sample at 298 K, a remnant magnetic field was reduced to less than 3 mOe using an ultra-low-field capability option. For convenience, this remnant field is hereafter denoted as the state $H = 0$.

(i) *DC magnetization*. The sample was cooled from 298 to 1.9 K at $H = 0$. After an external magnetic field (H) was applied at 1.9 K, the zero-field cooled magnetization (M_{ZFC}) was measured with increasing T from 1.9 to 60 K. The sample was kept at 70 K for 20 min. Then the field cooled magnetization (M_{FC}) was measured with decreasing T from 60 to 1.9 K.

(ii) *A hysteresis loop of DC magnetization*. The sample was cooled from 298 K to T (=1.9 or 3.3 K) at $H = 0$. Then DC magnetization at T was measured as H was varied from $H = 0$ to 1 kOe, from 1 to −1 kOe, and from −1 to 1 kOe in sequence.

(iii) *AC magnetic susceptibility* ($\chi = \chi' + i\chi''$). The sample was cooled from 298 to 1.9 K at $H = 0$. Then the dispersion χ' and absorption χ'' were simultaneously measured with increasing T from 1.9 to 20 K with and without H, where the frequency and amplitude of the AC magnetic field were $f = 1$ Hz and $h = 2$ Oe, respectively. After each T scan, H was changed at 30 K. The sample was cooled from 30 to 1.9 K. Then the measurement was repeated with increasing T from 1.9 to 20 K in the presence of H.

3. Results

3.1. χ' and χ''

Figures 1 and 2 show the T dependence of χ' for Pd-MG at various H, where $f = 1$ Hz and $h = 2$ Oe. The dispersion χ' at $H = 0$ slightly increases with decreasing T at the high-T side. It shows a peak at 3.8 K. Below 3.8 K, χ' drastically decreases with further decreasing T. The sign of χ' changes from positive to negative below 2.65 K. In contrast, the dispersion χ' for

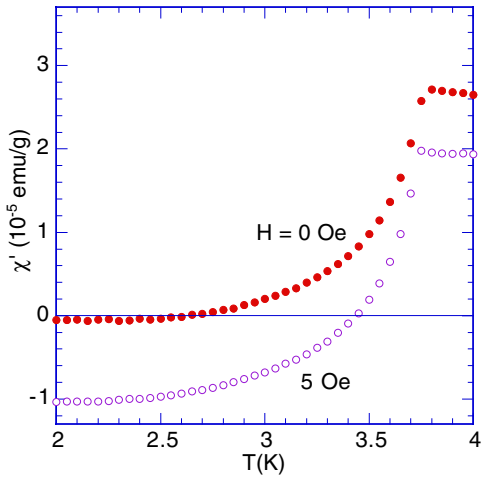

Figure 1. The T dependence of the dispersion χ' for Pd-MG at $H = 0$ and 5 Oe. $f = 1$ Hz. $h = 2$ Oe.

$5 \leqslant H \leqslant 350$ Oe still shows a positive peak, shifting to the low-T side with increasing H. However, the sign of χ' changes from positive to negative below a zero-crossing temperature T_0 (=3.45 K at $H = 5$ Oe). For $400 \leqslant H \leqslant 600$ Oe, no appreciable peak is observed in χ'. The dispersion χ' starts to decrease with decreasing T below T_0. The negative sign of χ' below T_0 for $H \geqslant 5$ Oe is related to the Meissner effect, giving some evidence of the superconductivity at low temperatures. We find that the derivative $\mathrm{d}\chi'/\mathrm{d}T$ shows a peak, shifting to the low-T side with increasing H. The peak temperature of $\mathrm{d}\chi'/\mathrm{d}T$ versus T is regarded as a superconducting transition temperature $T_c(H)$ $(=T_2(H))$ (see section 4.1 for the definition of $T_2(H)$). Using the value of χ' at 1.9 K ($\approx -2 \times 10^{-5}$ emu g^{-1}) and the density ρ which is of the order of 1–2 g cm^{-3} [7], the fraction of χ' relative to complete diamagnetism ($\chi_0 = -1/4\pi = -0.0796$ emu cm^{-3}) is estimated as only 0.05%, suggesting isolated superconducting islands.

Figure 3 shows the T dependence of the absorption χ'' in the presence of H. The data at $H = 0$ were presented in the previous paper [7]. The absorption χ'' at $H = 0$ increases with decreasing T. A drastic increase is observed around 3.5 K. In contrast, the T dependence of χ'' at $H \geqslant 20$ Oe is rather different from that at $H = 0$. It has a relatively sharp peak at a peak temperature. This peak shifts to the low-T side with increasing H. The peak temperature is the same as $T_2(H)$. We notice that the peak temperatures of χ' and χ'' at $H = 0$ are almost independent of AC frequency f for $0.07\ \mathrm{Hz} \leqslant f \leqslant 1$ kHz as have been reported in the previous paper [7].

3.2. M–H curve

Figure 4 shows the hysteresis loop of the DC magnetization $M(H)$ at $T = 1.9$ and 3.3 K, respectively. After the sample was cooled from 298 to 1.9 K at $H = 0$, the magnetization $M(H)$ was measured for $-1 \leqslant H \leqslant 1$ kOe. The magnetization curve at 1.9 K shows a non-typical hysteresis behaviour. There are some anomalies in the low-field region in the demagnetization and remagnetization curves at 1.9 and 3.3 K, which completely disappear at 5.5 K. In figures 5(a) and (b) we show the detail of the initial magnetization curve at 1.9 and 3.3 K. For the data at $T = 1.9$ K, the positive value of the initial magnetization M_{int} around

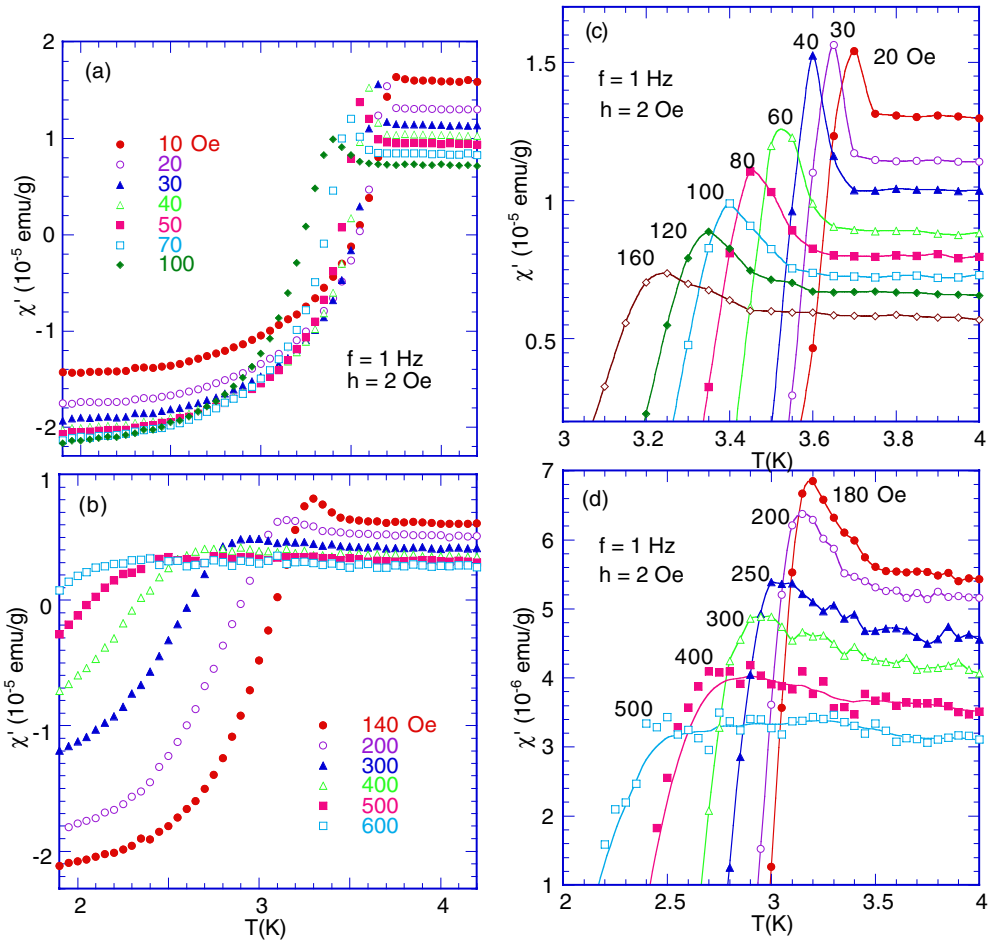

Figure 2. (a)–(d) The T dependence of χ' for Pd-MG at various H. $f = 1$ Hz. $h = 2$ Oe. The solid curves in (c) and (d) are guides to the eyes.

$H = 15$ Oe is sensitive to the condition of cooling from 298 to 1.9 K at $H = 0$. The negative value of $M_{\rm int}$ for $38 \leqslant H \leqslant 190$ Oe gives some evidence for the occurrence of the Meissner effect. The local-minimum field may be related to the lower critical field $H_{\rm c1}$. At 3.3 K this negative local minimum disappears.

3.3. IRM and TRM

Figure 6 shows the T dependence of the magnetization $M_{\rm ZFC}$, $M_{\rm IR}$, $M_{\rm FC}$, and $M_{\rm TR}$ for $H = 25$, 75, 150, and 200 Oe. The magnetization $M_{\rm IR}$ is the isothermal remnant (IR) magnetization. During the process of ZFC measurement (with increasing T), $M_{\rm ZFC}$ at each T was measured at H, and $M_{\rm IR}$ was measured at the same T 10^2 s later after setting H to zero. The magnetization $M_{\rm TR}$ is the thermoremnant (TR) magnetization. During the process of FC measurement (with decreasing T), $M_{\rm FC}$ at each T was measured at H, and $M_{\rm TR}$ was measured at the same $T10^2$ s later after setting H to zero. The magnetization $M_{\rm TR}$ is larger than $M_{\rm FC}$ and $M_{\rm IR}$ is larger than $M_{\rm ZFC}$ below a characteristic temperature T_α ($T_\alpha = 3.1$ K for $H = 75$ Oe),

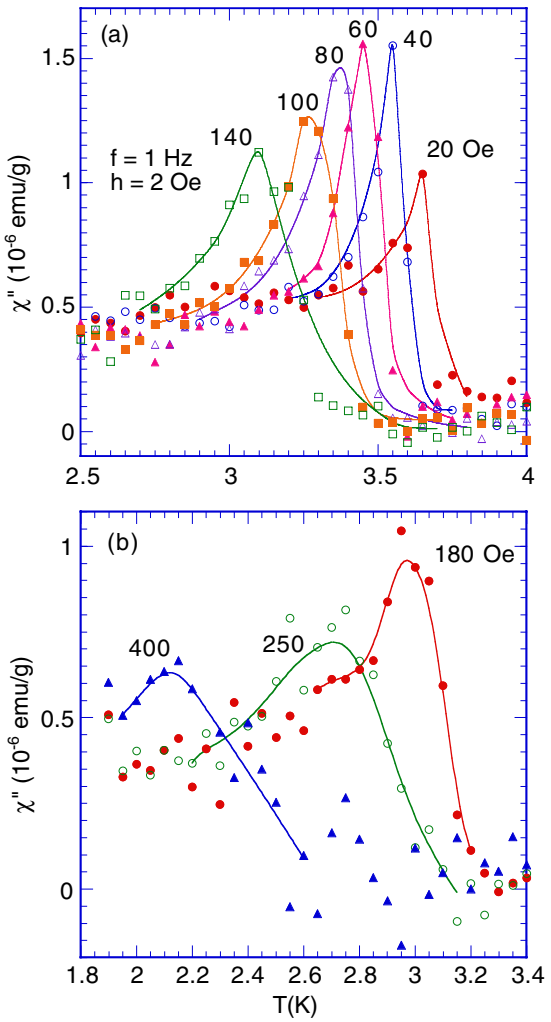

Figure 3. The T dependence of the absorption χ'' for Pd-MG at various H. $f = 1$ Hz. $h = 2$ Oe. The solid curves are guides to the eyes.

which are features common to the superconducting state. Similar behaviour of M_{TR} versus T and M_{FC} versus T has been reported in high-T_{c} superconductors La_2CuO_{4-y}:Ba [19] and $Bi_2Sr_2CaCu_2O_8$ [20, 21]. This is due to the flux trapping after switching off the field, giving a strong evidence of the superconductivity at low temperatures. The value of T_α is a little lower than $T_2(H)$: $T_2(H) = 3.34$ K at $H = 75$ Oe. Above T_α, M_{FC} is larger than M_{TR} and M_{ZFC} is larger than M_{IR}, which are features common to spin systems with spin frustration effects. The derivatives $\mathrm{d}M_{\mathrm{TR}}/\mathrm{d}T$ and $\mathrm{d}M_{\mathrm{IR}}/\mathrm{d}T$ at $H = 75$ Oe exhibit negative local minima at 3.34 and 3.45 K, respectively. The magnetization M_{TR} decreases with increasing T and reduces to a positive value above $T_2(H)$, suggesting the existence of magnetic short-range order. This is in contrast to the case of La_2CuO_{4-y}:Ba [19] and $Bi_2Sr_2CaCu_2O_8$ [20, 21]: M_{TR} becomes zero above $T_{\mathrm{c}}(H)$ $(=T_2(H))$, since no flux trapping occurs.

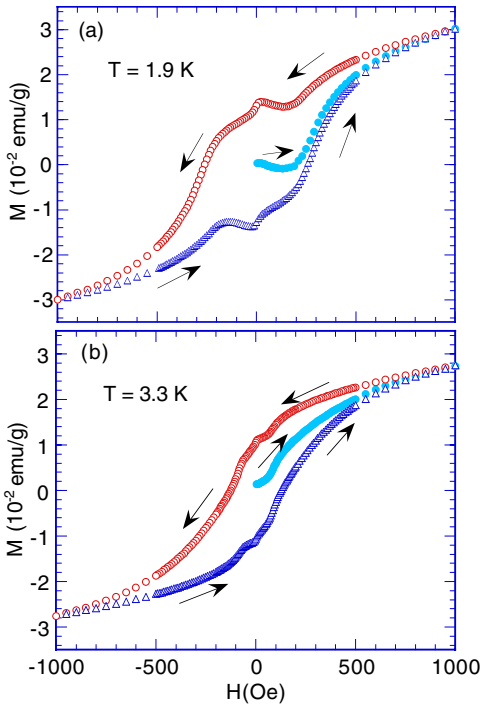

Figure 4. The hysteresis loop of the DC magnetization M for Pd-MG at (a) $T = 1.9$ K and (b) 3.3 K. After the sample was cooled from 298 to 1.9 K at $H = 0$, the measurement was made with increasing H from 0 to 1 kOe (closed circles), with decreasing H from 1 to -1 kOe (open circles), and with increasing H from -1 to 1 kOe (open triangles).

3.4. χ_{ZFC} *and* χ_{FC}

In the previous paper [7] we show the T dependence of χ_{ZFC} ($=M_{\mathrm{ZFC}}/H$) and χ_{FC} ($=M_{\mathrm{FC}}/H$) for Pd-MG where $H = 1$ Oe and $1.9 \leqslant T \leqslant 298$ K. We find that the deviation of χ_{ZFC} from χ_{FC} starts to appear below 298 K, suggesting a behaviour reminiscent of frustrated spin systems. In the present work, we have measured the T dependence of χ_{ZFC} and χ_{FC} at low temperatures below 6 K. Figures 7 and 8 show the T dependence of χ_{ZFC} and χ_{FC} for Pd-MG at various H. At $H = 1$ Oe (see figure 7), a cusp-like peak is observed at 3.8 K for both χ_{ZFC} and χ_{FC}. A local minimum is observed around 2.7 K in χ_{ZFC} and 3.4 K in χ_{FC}. As shown in figure 8, the cusp-like peak shifts to the low-T side with increasing H, becoming into a broader peak for $H \geqslant 100$ Oe. The local minimum of χ_{FC} at a temperature T_{min} also shifts to the low-T side with increasing H for $1 \leqslant H \leqslant 50$ Oe. The increase of χ_{FC} below T_{min} indicates the existence of magnetic short-range order at low temperatures. The resultant susceptibility arises from a competition between a negative diamagnetic susceptibility due to the Meissner effect and a positive susceptibility. Figure 9 shows the T dependence of the difference $\delta\chi$ defined by $\delta\chi = \chi_{\mathrm{FC}} - \chi_{\mathrm{ZFC}}$. The difference $\delta\chi$ provides a measure for the irreversible effect of magnetization. The difference $\delta\chi$ is positive at least below 60 K for $1 \leqslant H \leqslant 500$ Oe. The growth of the spin correlation length is greatly limited by the disordered nature of nanographites, forming magnetic short-range order. Note that $\delta\chi$ starts to increase drastically with decreasing T below a characteristic temperature T_δ, which is nearly equal to the peak temperature ($T_1(H)$) of χ' versus T (see section 4.1 for the definition of $T_1(H)$).

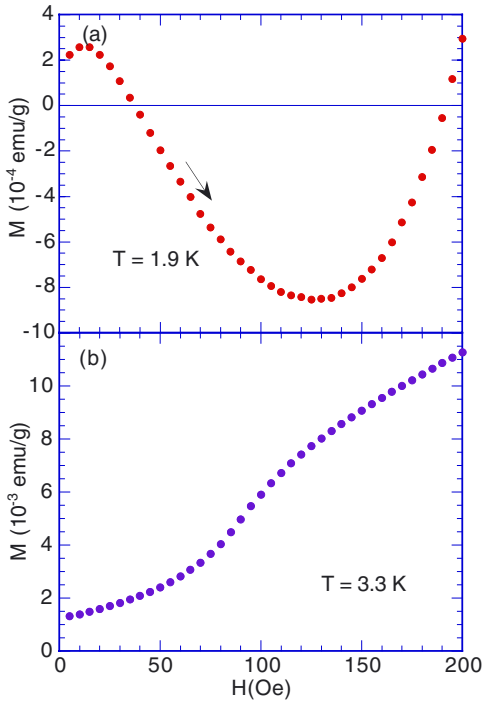

Figure 5. The H dependence of the DC magnetization M_{ZFC} for Pd-MG at (a) 1.9 K and (b) 3.3 K (closed circles). After the sample was cooled from 298 to 1.9 K at $H = 0$, the measurement was carried out with increasing H from 0 to 200 Oe. The data around $H = 0$ at 1.9 K are slightly different from those shown in figure 4.

Table 1. The Curie–Weiss constant C_g, Curie–Weiss temperature Θ, and T-independent susceptibility χ_0 determined from the least-squares fit of the data of χ_{FC} versus T at various H in the temperature range between 5 and 30 K.

H (Oe)	C_g (10^{-3} emu K g^{-1})	Θ (K)	χ_0 (10^{-5} emu g^{-1})
1	5.81	−6.9	4.02
5	3.85	−9.4	3.94
100	0.90	−13.1	3.72
200	0.53	−12.4	3.40
300	0.37	−11.5	3.47
400	0.28	−10.6	2.76
500	0.23	−9.8	2.63
3000	0.05	−5.4	0.66

3.5. DC magnetic susceptibility at high fields

Figure 10 shows the T dependence of χ_{FC} of Pd-MG for $H = 1 - 500$ Oe. Figure 11 shows the T dependence of χ_{FC} at $H = 3$ kOe. The susceptibility obeys the Curie–Weiss law only at low temperatures ($5 \leqslant T \leqslant 30$ K). The least-squares fit of the data χ_{FC} versus T for each H to

$$\chi_{FC} = \chi_0 + C_g/(T - \Theta) \tag{1}$$

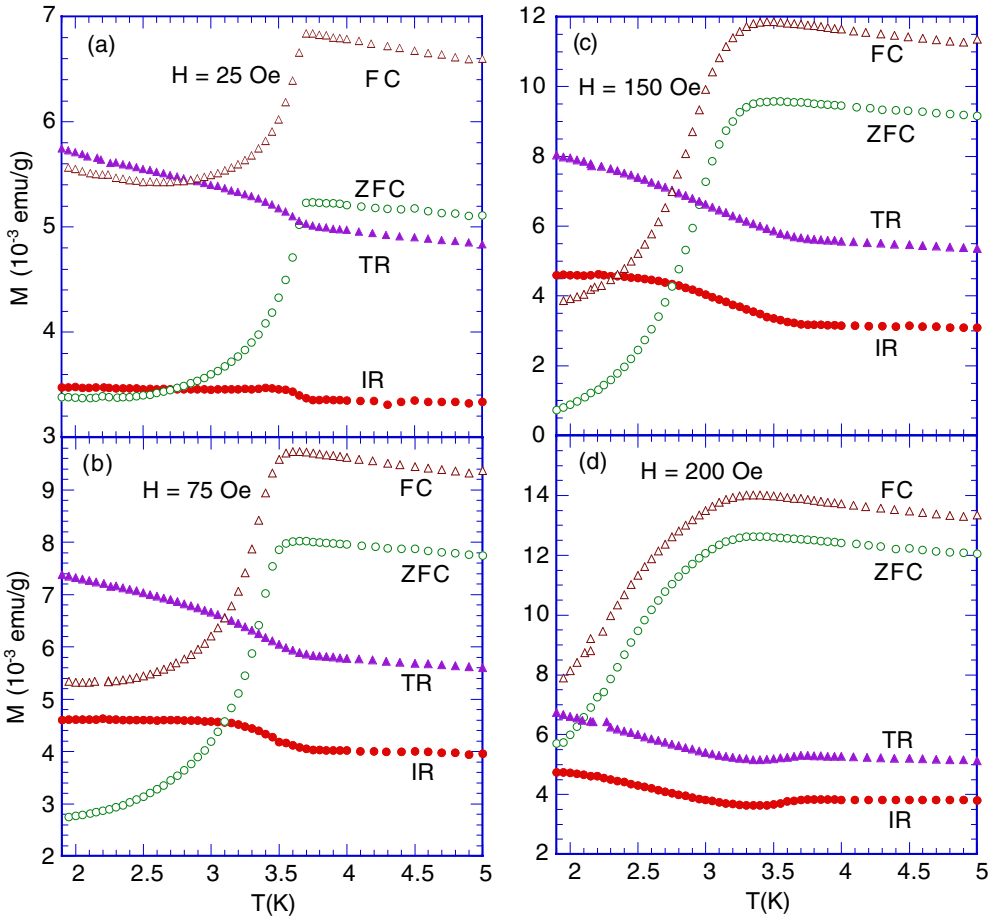

Figure 6. The T dependence of M_{ZFC}, M_{IR}, M_{FC}, and M_{TR} for Pd-MG. (a) $H = 25$, (b) 75, (c) 150, and (d) 200 Oe. During the ZFC measurement, M_{ZFC} at each T was measured at H and M_{IR} was measured 10^2 s later after H was set to zero field. During the FC measurement, M_{FC} at each T was measured at H. M_{TR} was measured 10^2 s later after H was set to zero field.

yields the Curie–Weiss constant C_{g}, the Curie–Weiss temperature Θ, and T-independent susceptibility χ_0, which are listed in table 1. The values of C_{g}, Θ, and χ_0 are different for different H. The inset of figure 11, and figure 12 show the T dependence of the corresponding reciprocal susceptibility $(\chi_{\mathrm{FC}} - \chi_0)^{-1}$ for $H = 3$ kOe, and $1 \leqslant H \leqslant 500$ Oe, respectively. We find that Θ is negative for any H, suggesting the AF nature of the system. The inclusion of the data for $T \geqslant 30$ K gives rise to a deviation of the data from (1). This is in contrast to the paramagnetic susceptibility due to magnetic impurities, where the agreement of the data with (1) becomes better as the data at higher T are included. Since Θ is close to zero, hereafter we call this behaviour Curie-like behaviour rather than Curie–Weiss-like behaviour. Such a Curie-like behaviour is due to the localized conduction electrons near zigzag edge sites of nanographites. Each electron has the effective magnetic moment $P_{\mathrm{eff}} = g[S(S+1)]^{1/2}$, where the Landé g factor $g = 2$ and spin $S = 1/2$ of the conduction electron. Then the value of N_{g}, the number of spins of localized conduction electrons (per gram), can be estimated as $N_{\mathrm{g}} = (3k_{\mathrm{B}}C_{\mathrm{g}}/\mu_{\mathrm{B}}^2 P_{\mathrm{eff}}^2) = 8.0 \times 10^{19}$ g^{-1}, where we use $P_{\mathrm{eff}} = \sqrt{3}$ and

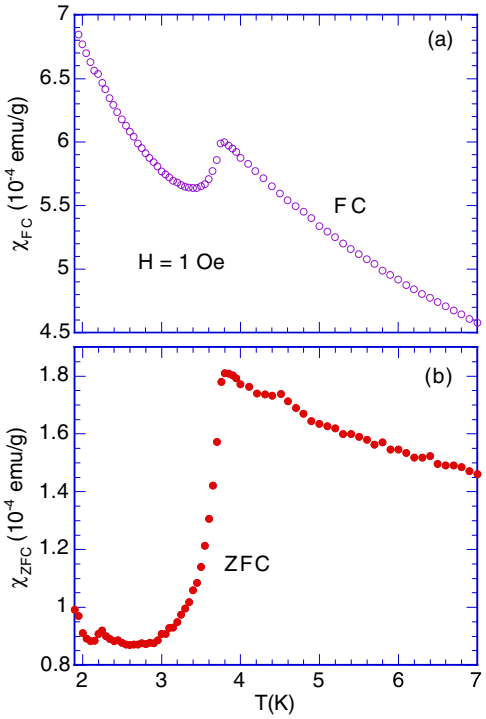

Figure 7. The T dependence of (a) χ_{ZFC} and (b) χ_{FC} for Pd-MG. $H = 1$ Oe.

$C_g = 4.98 \times 10^{-5}$ emu K g^{-1} for $H = 3$ kOe. This value of N_g is a little larger than that reported by Shibayama *et al* [22] for activated carbon fibres (ACF) composed of a disorder network of nanographites ($N_g = (0.39–4.2) \times 10^{19}$ g^{-1}).

Figure 13 shows the H dependence of M_{ZFC} at 1.9 K for $0 \leqslant H \leqslant 40$ kOe. The magnetization M_{ZFC} exhibits strong nonlinear H dependence, and it reaches 0.13 emu g^{-1} at $H = 40$ kOe, which does not correspond to the saturation magnetization M_s. It is predicted that the ratio of the saturation magnetization M_s ($=N_g \mu_B g S$) to C_g is given by $3k_B/[\mu_B g(S+1)]$, which is independent of N_g. When $g = 2$ and $S = 1/2$ for the conduction electron, the saturation magnetization M_s is estimated as 0.74 emu g^{-1}. This value of M_s is much larger than that of M_{ZFC} at $H = 40$ kOe. The reason for such a large M_s is not clear.

4. Discussion

4.1. The possibility of a quasi-2D superconductivity in Pd sheets

Our results obtained above are summarized in the H–T diagram of Pd-MG. In figure 14 we make a plot of the peak temperatures of χ' versus T, $d\chi'/dT$ versus T, χ'' versus T, $d\chi_{ZFC}/dT$ versus T, and $d\chi_{FC}/dT$ versus T, the local-minimum temperatures of $d\delta\chi/dT$ versus T and χ_{FC} versus T, and the characteristic temperature T_δ for $\delta\chi$ versus T, as a function of H. The data are classed in three groups:

(i) the upper line for χ' versus T and $\delta\chi$ versus T (denoted as the line $H_1(T)$ or the line $T_1(H)$),

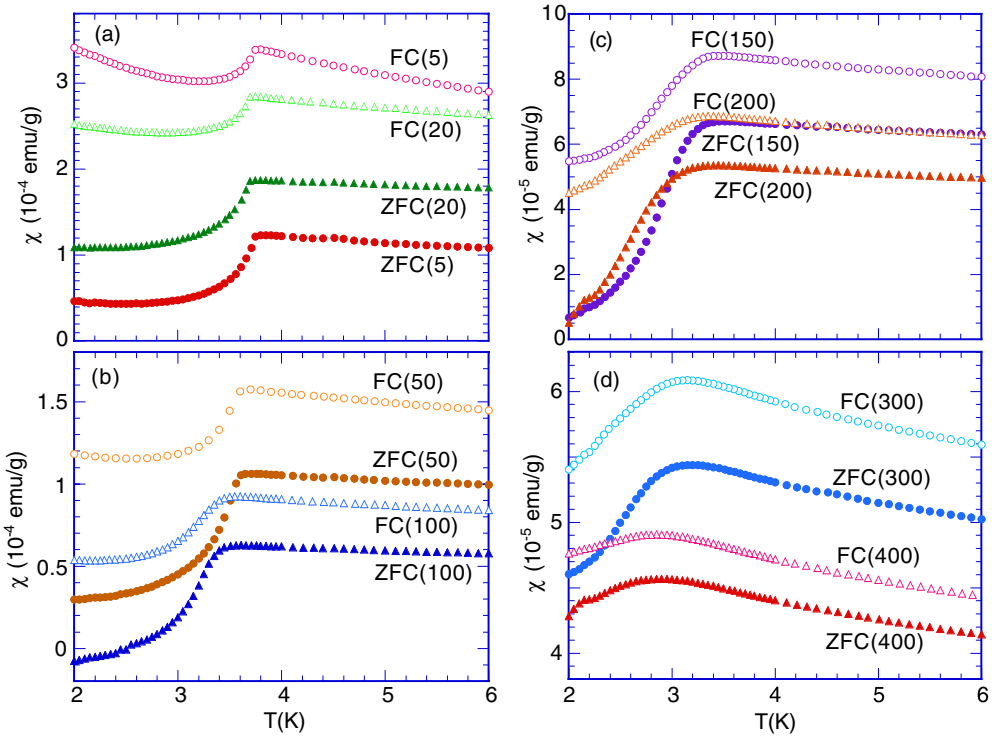

Figure 8. The T dependence of $\chi_{\rm ZFC}$ and $\chi_{\rm FC}$ for Pd-MG at various H.

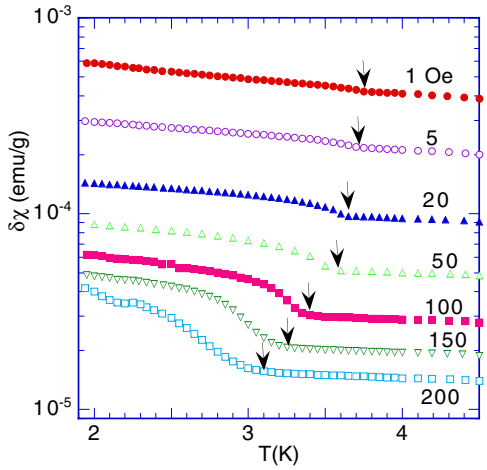

Figure 9. The T dependence of the difference $\delta\chi$ ($=\chi_{\rm FC}-\chi_{\rm ZFC}$) for Pd-MG at various H. The temperature (T_δ) denoted by arrow is a characteristic temperature at which $\delta\chi$ starts to increase drastically with decreasing T.

(ii) the intermediate line for $\mathrm{d}\chi'/\mathrm{d}T$ versus T, χ'' versus T, $\mathrm{d}\chi_{\rm ZFC}/\mathrm{d}T$ versus T, $\mathrm{d}\chi_{\rm FC}/\mathrm{d}T$ versus T, and $\mathrm{d}\delta\chi/\mathrm{d}T$ versus T (denoted as the line $H_2(T)$ or the line $T_2(H)$), and

(iii) the lower line for $\chi_{\rm FC}$ versus T which may correspond to the lower critical line $H_{\rm c1}(T)$ or the line $T_{\rm c1}(H)$.

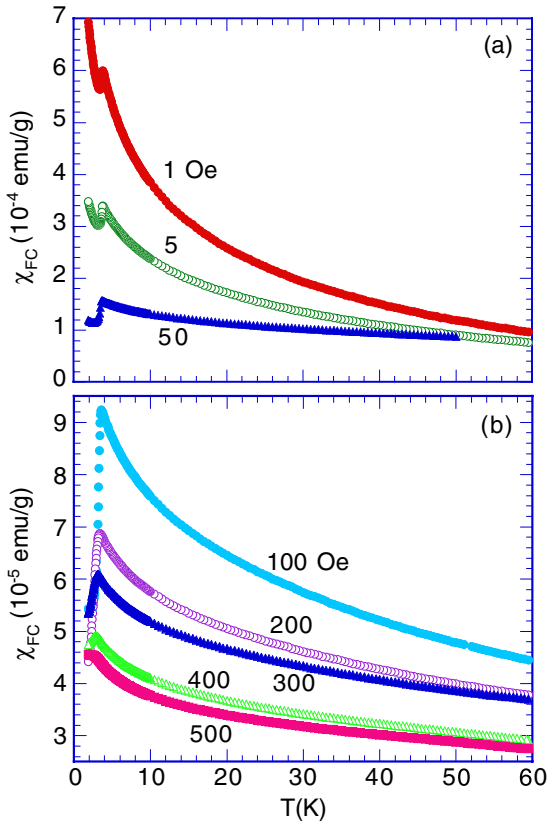

Figure 10. The T dependence of χ_{FC} for Pd-MG at various H.

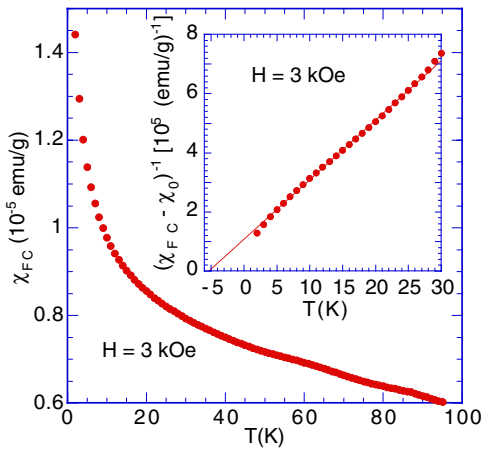

Figure 11. The T dependence of χ_{FC} for Pd-MG at $H = 3$ kOe. The inset shows the reciprocal susceptibility $(\chi_{FC} - \chi_0)^{-1}$.

Here we assume that the T dependence of the line H_j ($j = 1$ and 2) may be described by a power law form given by

$$H = H_j^*(1 - T/T_j)^{\alpha_j}, \tag{2}$$

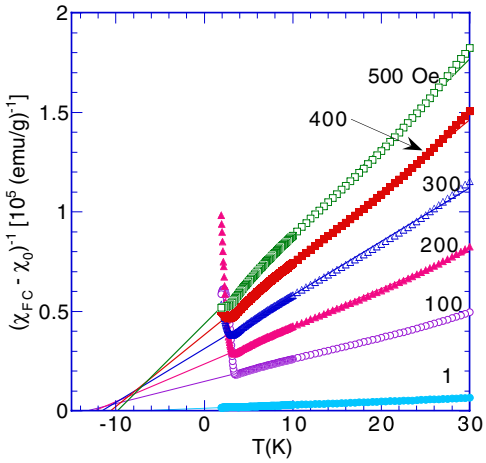

Figure 12. The T dependence of the reciprocal susceptibility $(\chi_{FC} - \chi_0)^{-1}$ for Pd-MG at various H, where χ_0 is a T-independent susceptibility determined from the least squares fit of the data to the Curie–Weiss law (1) for each H. The solid straight lines denote the fitting curves, where C_g, Θ, and χ_0 are listed in table 1.

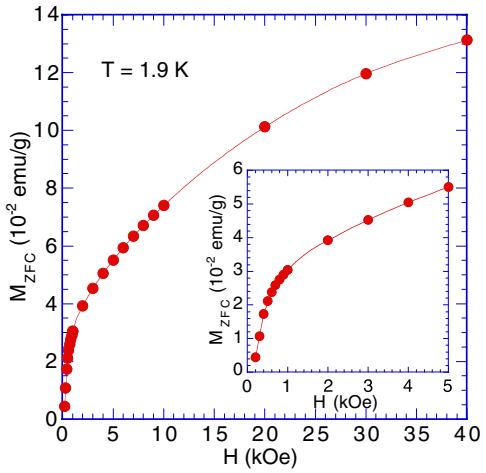

Figure 13. The H dependence of M_{ZFC} at 1.9 K for Pd-MG. After the sample was cooled from 298 to 1.9 K at $H = 0$, the measurement was carried out with increasing H from 0 to 40 kOe. The inset shows the detail of M_{ZFC} versus H at low H. The solid curves are guides to the eyes.

where α_j is an exponent, and H_j^* and T_j are the characteristic field and critical temperature, respectively. The least-squares fit of the data of H_1 versus T for $40 \leqslant H \leqslant 350$ Oe to (2) with $j = 1$ yields the parameters $\alpha_1 = 1.43 \pm 0.05$, $T_1 = 3.82 \pm 0.04$ K, and $H_1^* = 2.40 \pm 0.05$ kOe. The exponent α_1 is close to that (=1.50) for the irreversibility line (the so-called Almeida–Thouless (AT) line) [23]. In fact, as shown in figure 9, the difference $\delta\chi$ starts to increase with decreasing T below $T_1(H)$. The least-squares fit of the data of H_2 versus T for $0 \leqslant H \leqslant 450$ Oe to (2) with $j = 2$ yields the parameters $\alpha_2 = 1.06 \pm 0.07$, $T_2 = 3.63 \pm 0.04$ K, and $H_2^* = 1.12 \pm 0.04$ kOe. Note that the upper critical field H_{c2} of the type-II superconductor is defined by $H_{c2} = \Phi_0/(2\pi\xi^2)$, where Φ_0 (=2.0678×10^{-7} G cm^2) is a fluxoid and ξ is the coherence length [24]. Since ξ is proportional to $(1 - T/T_c)^{-1/2}$ according to the Ginzburg–Landau theory (mean-field theory), it is predicted that H_{c2} is proportional to $(1 - T/T_c)$ [24].

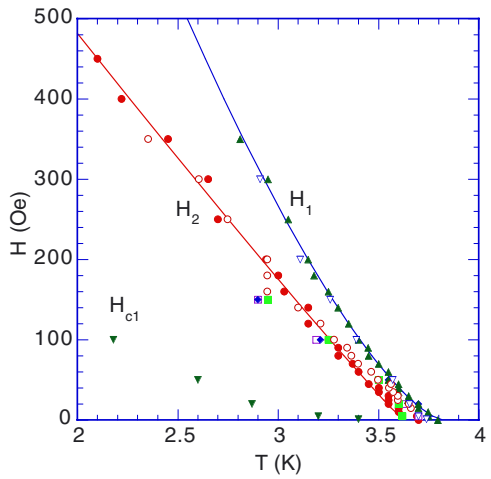

Figure 14. H–T diagram for Pd-MG, where the peak temperatures of χ' versus T (closed triangle), $\mathrm{d}\chi'/\mathrm{d}T$ versus T (closed circle), χ'' versus T (open circle), $\mathrm{d}\chi_{\mathrm{ZFC}}/\mathrm{d}T$ versus T (open square), and $\mathrm{d}\chi_{\mathrm{FC}}/\mathrm{d}T$ versus T (closed diamond), the local-minimum temperatures of $\mathrm{d}\delta\chi/\mathrm{d}T$ versus T (closed square) and χ_{FC} versus T (closed triangle down), and T_δ for $\delta\chi$ versus T (open triangle down), are plotted as a function of H. The superconducting transition temperature $T_{\mathrm{c}}(H)$ coincides with the peak temperatures ($T_2(H)$) of $\mathrm{d}\chi'/\mathrm{d}T$ versus T and χ'' versus T. The solid curves are least-squares fitting curves. See the text for further details.

The exponent α_2 is slightly larger than the mean-field value (=1). Thus it is reasonable to assume that T_2 coincides with T_{c}. In fact, $T_2(H)$ corresponds to a peak temperature of $\mathrm{d}\chi'/\mathrm{d}T$ versus T, which is defined as a critical temperature for usual superconductors. The upper critical field $H_{c2}(T = 0\ \mathrm{K})$ is roughly estimated from the slope of the line $H_2(T)$ at $T = T_{\mathrm{c}}$: $(-\mathrm{d}H_2/\mathrm{d}T)_{T_{\mathrm{c}}} = 180 \pm 20\ \mathrm{Oe\ K^{-1}}$. Using the relation $H_{c2}(0) \approx -0.69T_{\mathrm{c}}(\mathrm{d}H_2/\mathrm{d}T)_{T_{\mathrm{c}}}$ [25], the extrapolated $H_{c2}(0)$ is estimated as 450 ± 50 Oe. The coherence length $\xi(0)$ is estimated as $\xi(0) = 850 \pm 10$ Å, which is larger than the average size of Pd nanoparticles (=530 ± 340 Å).

It is well known that the H–T diagram of an ideal quasi-2D superconductors such high-T_{c} superconductors consists of a vortex lattice (Abrikosov lattice) phase, vortex glass phase, and a vortex liquid phase [26, 27]. The three lines (H_{al}, H_{ag}, and H_{gl}) merge into a multicritical point around T^* and H^*, where the line H_{al} is the boundary between the vortex lattice and the vortex liquid phase, the line H_{ag} is the boundary between the vortex lattice phase and the vortex glass phase, and the line H_{gl} is the boundary between the vortex glass phase and vortex liquid phase. Our H–T diagram of Pd-MG is compared with that of typical quasi-2D superconductors. It seems that the lines H_1 and H_2 correspond to the lines H_{gl} and H_{ag}, respectively. The line H_1 is the irreversibility line similar to the line H_{gl}. While the lines H_{gl} and H_{ag} merge at a multicritical point, the lines H_1 and H_2 do not merge even at $H = 0$. The absence of the multicritical point and the line H_{al} suggests that the superconductivity in Pd-MG is quasi-2D.

4.2. Magnetic short-range order in graphene sheets

The nature of the magnetic short-range order is now discussed. The existence of magnetic short-range order has been confirmed from the following results.

(i) The susceptibility χ_{FC} obeys a Curie–Weiss law with a negative Θ. The interactions between localized magnetic moments is antiferromagnetic.
(ii) The irreversibility between χ_{ZFC} and χ_{FC} occurs well above T_{c}.

The growth of spin order is greatly suppressed by the disordered nature of nanographites, forming the magnetic short-range order. Because of the frustrated nature of interaction between nanographites, no long-range order can develop at any finite temperatures. We have found several results supporting the magnetic short-range order below T_c. For an usual superconducting phase, M_{TR} is larger than M_{FC}, and M_{IR} is larger than M_{IR} below $T_c(H)$. For Pd-MG, M_{TR} is larger than M_{FC}, and M_{IR} is larger than M_{IR} for $T < T_\alpha < T_2(H)$, while M_{TR} is smaller than M_{FC}, and M_{IR} is smaller than M_{IR} for $T_\alpha < T < T_2(H)$. The latter is a feature common to the spin glass systems having a spin frustration effect.

Harigaya [15–17] has theoretically predicted that the magnetism in nanographites with zigzag edge sites depends on the stacking sequence of nanographites. For A–B stacking, there is no interlayer interaction J_1 at the edge site, where J_1 is the strength of the weak hopping interaction between neighbouring layers. This gives rise to the finite magnetic moment. The AF spin alignment is favourable for strong on-site repulsion U. The local magnetic moments tend to exist at the edge sites in each layer due to the large amplitude of the wavefunctions at these sites. The number of up-spin electrons is larger than that of down-spin electrons in the first layer. The number of down-spin electrons is larger than that of up-spin electrons in the second layer, and so on. The system can be described by the AF Heisenberg model with the exchange interaction J' $(=2J_1^2/U)$. For A–A type stacking, on the other hand, the magnetic moment per layer does not appear due to the interlayer interaction. The up- and down-spin electrons are not magnetically polarized in each layer. Although there is no detailed structural study on the stacking sequence in Pd-MG, the magnetic short-range order in Pd-MG may suggest that A–B stacking is dominant compared to A–A stacking. The spin correlation length along the c axis is considered to be of the same order as the nearest neighbour interlayer distance between nanographites. Since the Pd sheet is sandwiched between graphene sheets, there is no net molecular field on the Pd sheet from graphene sheets having A–B stacking along the c axis. This may lead to the coexistence of superconductivity and magnetic short-range order.

4.3. The effect of multilayered Pd sheets

In an ideal Pd-MG, there is one Pd sheet (monolayer) between adjacent graphene sheets. In reality, there is either a monolayer or multilayers (2–4 layers) between the graphene sheets. Multilayered Pd nanoparticles would generate internal stress inside the graphite lattice, leading to the break up of adjacent graphene sheets into nanographites. How does the spin fluctuation vary with the number of Pd layers in a quasi 2D-like Pd system consisting of stacked Pd layers? Bouarab *et al* [28] have predicted (i) no magnetic moment for $n = 1$, (ii) ferromagnetic moment for $n = 2$–5, and (iii) no magnetic moment for $n > 5$, where n is the number of Pd layers. The value of $N(E_F)$ for $n = 1$ is smaller than that in the bulk Pd. The 2D effect increases the DOS in the middle of the energy band, whereas it decreases the DOS in the higher energy side where E_F exists. Because the Stoner criterion $J_s N(E_F) > 1$ is not satisfied, the Pd monolayer is non-magnetic, where J_s is an exchange parameter. The peak of the DOS, which is much below E_F for $n = 1$, moves towards E_F for higher n. This prediction suggests that the Pd monolayer may be a superconductor because of the suppression of spin fluctuations. On the other hand, Pd layers with $n = 2$–5 may be a ferromagnet. In Pd-MG, at present it is not clear what is the minimum number of Pd layers (n_c) required for the ferromagnetic state. The value of n_c is dependent on the size of the Pd nanoparticles. However, it is reasonable to conclude that the Pd layers in Pd-MG are ferromagnetic for $n \geqslant n_c$ corresponding to the sample with the long-reaction time and are superconducting for $n < n_c$ corresponding to the sample with the short-reaction time [7].

5. Conclusion

Pd-MG undergoes a superconducting transition at T_c (=3.63 K). A quasi-2D superconductivity occurs in the Pd sheets. The magnetic short-range order appears well above T_c in the graphene sheets. The growth of the magnetic short-range order is limited by the disordered nature of nanographites. Further studies are required to understand the possible interplay between the superconductivity and the magnetic short-range order, including the nature of the irreversibility line $H_1(T)$.

Acknowledgments

The authors would like to thank K Harigaya for valuable discussions on antiferromagnetism in nanographites. The work at Binghamton was supported by the Research Foundation of SUNY-Binghamton (contract number 240-9522A). The work at Osaka (JW) was supported by the Ministry of Education, Science, Sports and Culture, Japan (the grant for young scientists (No 70314375)) and by Kansai Invention Centre, Kyoto, Japan.

References

[1] Nagarajan R, Mazumdar C, Hossain Z, Dhar S K, Gopalakrishnan K V, Gupta L C, Godart C, Padalia B D and Vijayaraghavan R 1994 *Phys. Rev. Lett.* **72** 274–7
[2] Cava R J, Takagi H, Batlogg B, Zandbergen H W, Krajewski J J, Peck W F Jr, van Dover R B, Felder R J, Siegrist T, Mizuhashi K, Lee J O, Eisaki H, Carter S A and Uchida S 1994 *Nature* **367** 146–7
[3] Walter J and Shioyama H 1999 *Phys. Lett.* A **254** 65–71
[4] Walter J 2000 *Adv. Mater.* **12** 31–3
[5] Walter J 2000 *Phil. Mag. Lett.* **80** 257–62
[6] Walter J, Heiermann J, Dyker G, Hara S and Shioyama H 2000 *J. Catal.* **189** 449–55
[7] Suzuki M, Suzuki I S and Walter J 2000 *Phys. Rev.* B **62** 14171–80
[8] Fay D and Appel J 1977 *Phys. Rev.* B **16** 2325–8
[9] Papaconstantopoulos A and Klein B M 1975 *Phys. Rev. Lett.* **35** 110–3
[10] Pinski F J, Allen P B and Butler W H 1978 *Phys. Rev. Lett.* **41** 431–4
[11] Stritzker B 1979 *Phys. Rev. Lett.* **42** 1769–73
[12] Meyer J D and Stritzker B 1982 *Phys. Rev. Lett.* **48** 502–5
[13] Fujita M, Wakabayashi K, Nakada K and Kusakabe K 1996 *J. Phys. Soc. Japan* **65** 1920–3
[14] Wakabayashi K, Fujita M, Ajiki H and Sigrist M 1999 *Phys. Rev.* B **59** 8271–82
[15] Harigaya K 2001 *J. Phys.: Condens. Matter* **13** 1295–302
[16] Harigaya K and Enoki T 2002 *Chem. Phys. Lett.* **351** 128–34
[17] Harigaya K 2001 *Chem. Phys. Lett.* **340** 123–8
[18] See for example Enoki T, Suzuki M and Endo M 2003 *Graphite Intercalation Compounds and Applications* (New York: Oxford University Press)
[19] Müller K A, Takashige M and Bednorz J G 1987 *Phys. Rev. Lett.* **58** 1143–6
[20] Papadopoulou E L, Nordblad P, Svendlindh P S, Schöneberger R and Gross R 1998 *Phys. Rev. Lett.* **82** 173–6
[21] Papadopoulou E L and Nordblad P 2001 *Eur. Phys. J.* B **22** 187–91
[22] Shibayama Y, Sato H, Enoki T and Endo M 2000 *Phys. Rev. Lett.* **84** 1744–7
[23] de Almeida J R L and Thouless D J 1978 *J. Phys. A: Math. Gen.* **11** 983–90
[24] See, for example Ketterson J B and Song S N 1998 *Superconductivity* (Cambridge: Cambridge University Press)
[25] Werthamer N R, Helfand E and Hohenberg P C 1966 *Phys. Rev.* **147** 295–302
[26] Blatter G, Feigel'man M V, Geshkenbein V B, Larkin A I and Vinokur V M 1994 *Rev. Mod. Phys.* **66** 1125–388 see also references therein
[27] Gammel P L, Huse D A and Bishop D J 1998 *Spin Glasses and Random Fields* ed A P Young (Singapore: World Scientific) pp 299–320
[28] Bouarab S, Demangeat C, Mokrani A and Dreyssé H 1990 *Phys. Lett.* A **151** 103–5